

Improved non-contact 3D field and processing techniques to achieve macrotexture characterisation of pavements



Vikki Edmondson^{a,*}, John Woodward^a, Michael Lim^a, Malal Kane^b, James Martin^a, Islam Shyha^a

^a Department of Mechanical and Construction Engineering, Northumbria University, Ellison Place, Newcastle Upon Tyne NE1 8ST, United Kingdom

^b IFSTTAR-Nantes, Institut Français des Sciences et Technologiques des Transports, de l'Aménagement et des Réseaux Allée des Ponts et Chaussées Route de Bouaye – CS4, 44344 Bouguenais Cedex, France

HIGHLIGHTS

- Paper scrutinizes accuracy of non-contact techniques to characterise macrotexture.
- Structure from Motion (SfM) photogrammetry successfully measures S_q , representing pavement texture depth.
- The Nyquist of Terrestrial Laser Scanners and SfM techniques generates potential to measure microtexture.
- Functional areal parameters Spd and Spc are sensitive to sample size.
- Wider scale approaches are required to capture functional areal parameters for road surfaces.

ARTICLE INFO

Article history:

Received 16 April 2019

Received in revised form 4 August 2019

Accepted 8 August 2019

Available online 28 August 2019

Keywords:

Pavement texture

Macrotexture

Skid resistance

Structure from Motion (SfM)

Terrestrial Laser Scanning (TLS)

ABSTRACT

Macrotexture is required on pavements to provide skid resistance for vehicle safety in wet conditions. Increasingly, correlations between macrotexture measurements captured using non-contact techniques and tyre-pavement contact friction are being investigated in order to enable more robust and widescale measurement and monitoring of skid resistance. There is a notable scarcity of research into the respective accuracy of the non-contact measurement techniques at these scales. This paper compares three techniques: a laser profile scanner, Structure from Motion photogrammetry and Terrestrial Laser Scanning (TLS). We use spectral analysis, areal surface texture parameters and 2D cross-correlation analysis to evaluate the suitability of each approach for characterising and monitoring pavement macrotexture. The results show that SfM can produce successful measures of the areal root mean square height (S_q), which represents pavement texture depth and is positively correlated with skid resistance. Significant noise in the TLS data prevented agreement with the laser profiler but we show that new filtering procedures result in significantly improved values for the peak density (Spd) and the arithmetic peak mean curvature (Spc), which together define the shape and distribution of pavement aggregates forming macrotexture. However, filtering the TLS data results in a trade-off with vertical accuracy, thus altering the reliability of S_q . Finally, we show the functional areal parameters Spd and Spc are sensitive to sample size. This means that pavement specimen size of 150 mm × 150 mm or smaller, when used in laboratory or field observations, are inadequate to capture the true value of areal surface texture parameters. The deployment of wider scale approaches such as SfM and spectrally filtered TLS are required in order to successfully capture the functional areal parameters (Spc and Spd) for road surfaces.

© 2019 The Authors. Published by Elsevier Ltd. This is an open access article under the CC BY license (<http://creativecommons.org/licenses/by/4.0/>).

1. Introduction

Adequate texture on the surface of a pavement is required to provide skid resistance or friction at the tyre/road interface for vehicle safety in wet conditions [1–4]. Skid resistance is also influenced by temperature, presence of contaminants, speed and tyre tread thickness [5]. Friction forces generated from the contact of the tyre with texture are a consequence of the viscoelastic deformation of the tyre, and increase in dry conditions with adhesion

* Corresponding author.

E-mail addresses: vikki.edmondson@northumbria.ac.uk (V. Edmondson), john.woodward@northumbria.ac.uk (J. Woodward), michael.lim@northumbria.ac.uk (M. Lim), malal.kane@ifsttar.fr (M. Kane), james.e.martin@northumbria.ac.uk (J. Martin), islam.shyha@northumbria.ac.uk (I. Shyha).

[6]. Pavement texture is defined as the deviation of the pavement surface from a true planar surface [7] and has been characterised at different scales according to the wavelengths of the deviations [8]. Microtexture suspected to induce adhesion, represents the texture components with wavelengths from less than 0.5 mm and peak amplitude from 0.001 to 0.5 mm. Microtexture correlates to the asperities upon the surface of coarse road aggregates [9], and also to the fine particles present in the mixture constituting the wearing course of the pavement. In wet conditions, adhesion is reduced by the phenomenon of viscoplaning [6], where a degree of tyre contact is lost with the pavement due to the presence of a thin water film (in the order of a tenth of a millimetre or less). Macrotexture, suspected to induce hysteresis response in the viscoelastic tyre, represents the texture components with wavelengths from 0.5 mm to 50 mm and amplitude of 0.1 mm to 20 mm (formed by the shape, size and gradation of road aggregates on a pavement surface). Macrotexture acts also to disperse water, under wet conditions, through the gaps in between the road aggregates [10]. Thus, macrotexture, has been shown to influence the way skid resistance reduces with increasing speed in wet conditions [11]. Generally, with equal microtexture, pavement surfaces with higher macrotexture offer more friction resistance as speed increases than pavements with lower macrotexture under the same contact conditions [12,13].

Thus, the preservation of adequate skid resistance requires the monitoring of macrotexture [1] to ensure sufficient texture remains on the pavement to prevent skidding. Standard monitoring techniques involve either a sand patch test [14] or a direct measurement of the frictional resistance through a rubber pad [15] or test wheel making contact with a wetted pavement [16,17]. Kogbara et al. [18] provide a full summary of devices and their operating principles. These contact devices are known to be susceptible to seasonal variation [19]. This phenomenon has been attributed to a number of factors: the sensitivity of rubber resilience to temperature change [20]; changes induced by temperature in the viscosity of the test water of a device [21]; and differential polishing of the aggregate microtexture throughout the year [22]. Survey results obtained from these devices require statistical interpretation [1,23] with individual devices requiring harmonisation with the rest of a fleet [24]. Friction measurements from rubber contact base devices are also known to be susceptible to changes in travel speed [25]. Direct comparison between different devices adopted in particular countries is also difficult, as measurements are influenced by machine operating conditions such as the load, speed, slip ratio and the composition of the rubber.

The problems associated with contact measurement techniques, make a reliable non-contact technique desirable. Accurate non-contact macrotexture measurement is one step towards the estimation of pavement friction values via analytical modelling [5,26–28]. Researchers have successfully deployed contactless techniques under laboratory conditions to measure texture; typically to a size of 100 × 100 mm [29,30]. At present, there are also a number of in-situ proprietary spot contactless techniques available for use in the field, including the Circular Texture Meter [31], the Model 9300 laser texture scanner [32] and close-range stereo photogrammetry [33–35], which requires a minimum of three images taken from different perspectives to reconstruct a 3D pavement surface. These techniques offer an alternative to the simple sand patch test [14,36,37], where a measured volume of fine material is spread in a circular motion into a road's surface depressions to find the mean texture depth, for in-situ localised pavement texture assessment. Recent research, focused on the development of a prototype test rig [38] adopting a laser range finder, that uses triangulation, to measure texture in the field or to detect defect on pavements [39], but is still restricted to a localised area comparable to that of a sand patch test. The minimum texture

profile height measured by the rig was limited to 0.032 mm, with a spatial sampling frequency of about 4 mm⁻¹, thus meeting only part of the range needed for macrotexture. 3D handheld scanners [40,41], using triangulation principles, have also been deployed to capture macrotexture in-situ [42]. These scanners are designed for metrology applications, and having a limited field of view, lack scalability. Advances in 'off-the-shelf' laser and photogrammetry technology and point cloud post-processing applications means there is now the potential to capture macrotexture over larger areas, potentially more representative areas using contactless techniques. Terrestrial Laser Scanning (TLS) offers rapid, full 3D high resolution reconstruction of a highway surface as a point cloud [43] and Structure from Motion (SfM) photogrammetry [44,45] offers a low-cost method utilising digital images to generate a 3D dense point cloud data of surfaces.

This paper introduces a method to characterise macrotexture using TLS and SfM over a typical full lane width. Recent research [34] suggests that frictional resistance is sensitive to certain areal parameters [46,47] (Table 1). Particularly, to the density of peaks within the macrotexture of a highway surface, S_{pd} , and to the pointiness or arithmetic mean of the principal curvature of the same peaks S_{pc} ; which together characterise the shape and size of the road aggregates. Furthermore, the areal parameters root mean square of surface departures, S_q , as the standard deviation of peak height from an average plane, is spatially equivalent to mean profile depth [48]. Mean profile depth represents the averaged values over an overall 2D profile length, of the difference within a lateral distance (typically in the order of a tyre/pavement contact) between the profile and a horizontal line through the top of the highest peak. This paper explores the accuracy of the scalable TLS

Table 1

Areal surface texture parameters used to characterise macrotexture. Parameters are defined by ISO 25178 [51]. S_q the root mean square of surface departures, and the linked parameters S_p and S_v (maximum peak and pit height) are equivalent to mean texture depth used at present to evaluate macrotexture, principally by means of the volumetric patch techniques. S_{pd} represents the density of the peaks of the road aggregate on the pavement surface and S_{pc} is a measure of the principal curvature of the peaks, characterising the shape and size of the road aggregates.

Parameter Symbol	Parameter Name	Description	Calculation Equation
S_q	Root mean square height	Root mean square value of the surface departures within the sampling area.	$S_q = \sqrt{\frac{1}{A} \iint_A Z^2(x, y) dx dy}$
S_{sk}	Skewness	Defines the shape of topography height distribution as a measure of symmetry about the mean line.	$S_{sk} = \frac{1}{S_q^3} \left[\frac{1}{A} \iint_A Z^3(x, y) dx dy \right]$
S_p	Maximum peak height	Largest peak height within a definition area A .	S_p
S_v	Maximum pit height	Smallest pit height value within a definition area.	S_v
S_{pd}	Peak density	The number of peaks per unit area.	$S_{pd} = \frac{N}{A}$
S_{pc}	Arithmetic mean peak curvature	Measure of the principal curvature of the peaks.	$S_{pc} = -\frac{1}{2} \frac{1}{n} \sum_{k=1}^n \left(\frac{\partial^2 z(x, y)}{\partial x^2} + \frac{\partial^2 z(x, y)}{\partial y^2} \right)$

and SFM approaches to determining these measurements in comparison to measurements achieved using a 3D Smart Laser Profile Sensor [49]. The 3D Smart Laser Profile Sensor was selected as an accurate well-constrained controlled dataset of 2D profile macrotexture measurements from which to formulate a 3D surface, as such laser profile sensors are well-understood have been deployed widely previously to capture 2D profile measurements of macrotexture [50–52]. This paper will first introduce the methods applied to capture point cloud data in the field using the three techniques, before rigorously considering the accuracy of results obtained through the application of spectral analysis, areal parameters and 2D cross-correlation.

2. Methods

2.1. Remote sensing technology

2.1.1. Terrestrial Laser scanning

The TLS data were collected using the Faro Focus 3D X Series phase-based laser scanner on a tripod mounted inverted as shown in Fig. 1a. The static scanner was set-up at a height of 1 m above the pavement surface on a levelled tripod, and the desired scanning parameters were entered on the instrument's home screen. Fig. 2 details the workflow for programming the scanner's settings prior to completing a scan. To retain a practical completion time for the survey, a resolution of 1/5 and quality of 6× was adopted, providing a scan time of 22.38 min. The scanner stores data on a SD memory card, and this was post processed using Faro Scene 7.1 software to extract, register and align the point cloud.

2.1.2. Structure from Motion photogrammetry

Static digital images (5472×3648 pixels) were captured at the test location using a digital single-lens reflex camera with 50 mm fixed focal length, mounted on a camera tripod and dolly (refer to Fig. 1b). Following the method of [34] a minimum of 60% forward overlap and 30% sideways overlap between photographs was maintained. Previous research [45] has demonstrated that capturing flat surfaces using SfM with predominantly parallel images, and adopting self-calibration of camera locations can cause

deformation of the point cloud typified by 'doming' effects. To prevent these affects, over lapping photographs, were captured at three heights (500 mm, 600 mm and 750 mm) above the pavement surface, across the width of the highway (Fig. 3a).

Agisoft Photoscan version 1.3.4.5067 software 6 was used to post process the images enabling reconstruction of the overlapping photographs into a 3D point cloud. The software determines the position and orientation of cameras automatically using a scale invariant feature transform (SIFT) [44]. The SIFT matches up identified features across the image set, to establish their 3D coordinates and generate a sparse cloud. The sparse cloud is then densified into a dense point cloud by the software using Multi View Stereo techniques [53]. Fig. 3 illustrates the key stages of the construction of a point cloud from the camera images. Using this approach, an area equivalent to the width of a standard road lane (3.65 m) was successfully reconstructed without deformation.

2.1.3. 3D smart laser profiling

The 3D Smart Laser Profile Sensor, an LMI Technologies Gocator 2350, was mounted upon a trolley at a height of 500 mm (Fig. 1c) and powered by a 60-volt battery. One trolley wheel made contact with a digital quadrature encoder fitted to a 200 mm circumference measuring wheel. The digital encoder was wired to provide a pulse signal to the 3D Smart Sensor, being programmed to produce 40,000 pulses per rotation of the measuring wheel. Each pulse equates to a travel distance of 0.005 mm and this information is used to enable 3D surface profiles to be captured at variable speed. The 3D Smart Laser Profile Sensor's settings were programmed using Gocator Emulator version 4.6.7.17 software, installed on a conventional laptop. Fig. 2b details the workflow for programming the 3D Smart Laser Profile Sensor's settings prior to completing a scan. The data were collected at walking speed every 201 pulses or 1.005 mm over a 3 m section, with the 3D Smart Laser Profile Sensor operating at a typical field of view width of 300 mm. The 3D Smart Laser Profile Sensor, is equipped with the capacity to view the laser points forming the profile line on the highway surface in 'real-time'. This facilitates adjustment of the laser exposure level and active measurement area to accommodate ambient light levels, stray light and variability of highway surface reflectivity.



Fig. 1. Equipment set-up for: (a) Terrestrial Laser Scanner. The Faro Focus 3D X Series scanner is fitted onto a tripod stand (i) using an invert head fitting (ii). (b) Structure from Motion. A digital single-lens reflex camera with 50 mm fixed focal lens (iii), is mounted on a standard Leica camera tripod (iv) and dolly (v). (c) 3D Smart Laser Profile Sensor. LMI Technologies Gocator 2350 laser profile sensor (vi) is fixed at a height of 500 mm to the trolley frame and operated using Gocator Emulator version 4.6.7.17 software installed on a standard laptop (vii). A quadrature digital encoder fitted to a 200 mm measuring wheel (viii) enables images to be captured at variable speed up to a maximum of 10 km/h. The system is powered by a 60-volt battery (ix).

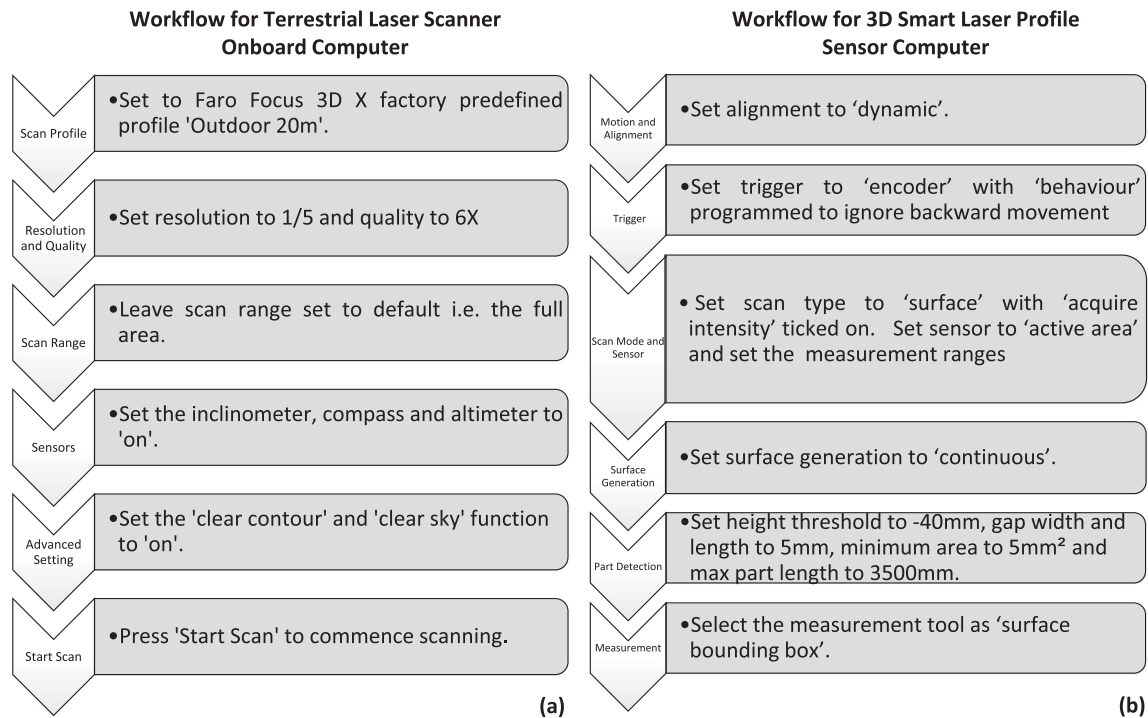


Fig. 2. (a) Workflow for programming both the Faro Focus 3D X Series Terrestrial Laser Scanner's onboard computer the LMI Technologies Gocator 2350 3D Smart Laser Profile Sensor prior to completing a scan. The Faro Focus 3D X Series Terrestrial Laser Scanner's onboard computer is accessed via the scanner's main touch screen display, housed within the head of the instrument. Key settings are accessed by selecting the 'Parameters' button on the 'Home' screen. Key setting requirements illustrated by the vertical arrows (left of figure) were adjusted in accordance with the instruction presented in the grey box (right of figure). The LMI Technologies Gocator 2350 3D Smart Laser Profile sensor computer is programmed using Gocator Emulator version 4.6.7.17 software, installed on a conventional laptop. Key settings are accessed by selecting the 'Manage' or 'Scan' buttons from the software's top toolbar. Key setting requirements illustrated by a vertical arrows (left of figure) were adjusted in accordance with the instruction presented in the grey box (right of figure).

The surface profiles extracted from the 3D Smart Laser Profile Sensor were post processed using Gocator_Emulator version 4.6.7.17 and kCSVConverter software to an ASCII xyz file format suitable for point cloud post processing [54].

2.2. Test location

To test the three techniques a field site was selected that contained three standard types of pavement surface within close proximity (Fig. 4), allowing for the same ambient conditions to be assumed over the surfaces. The site included a close graded dense bitumen macadam (DBM), and a gap graded hot rolled asphalt (HRA), as well as surface dressing (SD). Test were undertaken on the dry pavement surfaces with permanent ground control points being installed to demarcate each surface using 16 mm survey nails.

2.3. Deriving macrotecture parameters from non-contact survey techniques

The 3D point cloud data for the DBM, HRA and SD surfaces were captured consecutively on the same day using the three different techniques. The point clouds obtained from each technique were then aligned utilising the installed reference ground control points in Cloud Compare v 2.10 software [55], to facilitate direct comparison between the surfaces. Subsequently, 150 mm × 150 mm sample areas (representing a typical laboratory specimen size) were clipped for each surface from the aligned point clouds for analysis. These clipped point clouds were then loaded into MountainsMap Premium version 7.4 and the software used to remove any transverse or longitudinal slope by method of least squares, and to calculate the standard areal parameters as listed in Table 1, to

characterise the macrotecture. Areal parameters were adopted, in contrast to 2D profile parameters [56], as these are recognised as providing a more complete description of a surface [46], capturing height with respect to both the 'x' and 'y' direction to characterise functional aspects such as texture, shape and direction. In sampling the point cloud data to make successful areal measurements it is important that Nyquist values be smaller than the smallest desired surface macrotecture requiring characterisation. Nyquist sampling theorem states that the shortest wavelength that can be defined from a digital dataset is two digital sample intervals long. Therefore, the wavelength or sample length available to characterise pavement texture areal parameters, is defined by the relationship between point cloud density and sample size.

2.4. Deriving 2D wavenumber amplitude spectra from non-contact techniques and filtering

Image datasets can be analysed by MATLAB software to transform them to the wavenumber domain, allowing images to be characterised by spatial frequency. Accordingly, 2D Kx-Ky wavenumber spectral analyses of the samples [56] were calculated in MATLAB to determine the areal wavenumber characteristics of the surfaces captured using the different techniques. To prevent spectral leakage caused by discontinuities at the edges of each measured sample area, the amplitude of the signal at the outer edges was attenuated using a cosine taper Tukey window that extended for 10% from the extreme edges of the sample line [57]. The resulting 2D wavenumber spectra enabled the wavenumber content of the data to be determined, which facilitated the selection of an appropriate 2D wavenumber filter to attenuate high wavenumber noise from the macrotecture signal.

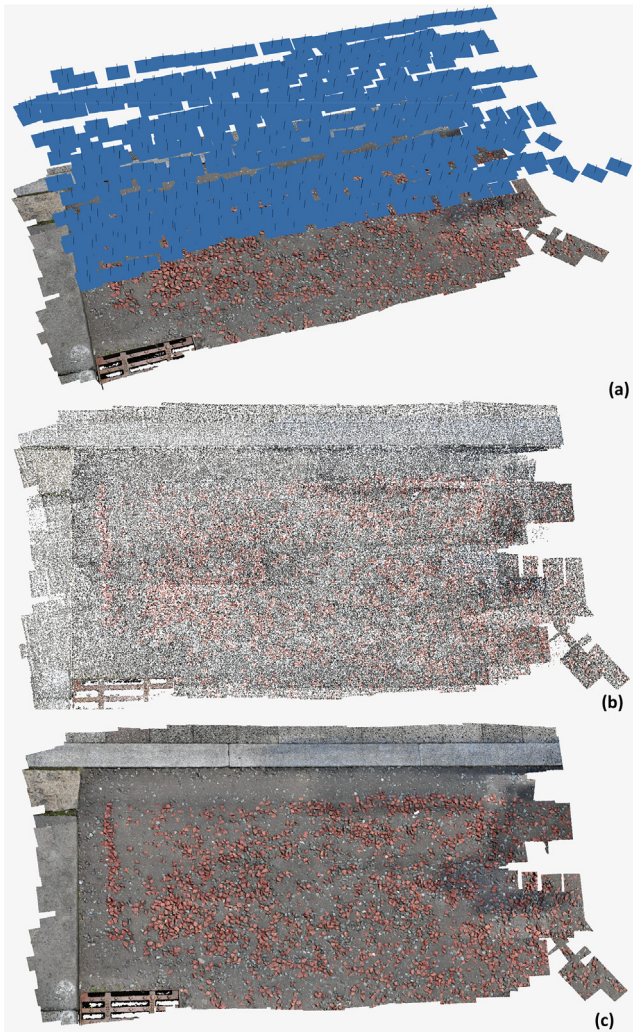


Fig. 3. Key Stages of construction of a scaled point cloud reconstruction from digital images. The surface modelled is a Hot Rolled Asphalt with 20 mm red chipping. (a) The camera position take for each photograph image, (indicatively represented in the figure by the blue rectangles (i.e. not to scale)) are calculated in Agisoft Photoshop. The camera images are captured in the field at three independent heights, typically 500 mm, 600 mm and 750 mm, with a minimum of 60 percent forward overlap and 30 percent sideways overlap between images. (b) 3D coordinates for key features across the aligned photograph image set are determined and used to construct points in a sparse point cloud. (c) The sparse point cloud is used to generate a dense point cloud in Agisoft Photoshop. The final dense cloud is scaled using known ground control points measurements established in the field.

Examining the spectra for each non-contact technique the 3D Smart Laser Profile Sensor was the lowest resolution technique, containing wavenumbers not greater than 0.1 mm^{-1} . Consequently, to achieve conformity of the wavelengths for areal parameter analysis across techniques a wavenumber filter of 0.1 mm^{-1} was applied to the SfM and TLS data. A low pass zero phase Butterworth wavenumber filter [57] was then designed to remove high wavenumber noise components from the data, up to the Nyquist wavenumber [58]. The filter was applied in a two-pass process, firstly for every trace in the x-direction and then the y-direction, thus creating a 2D filtered data set. Normalised 2D autocorrelations and cross-correlation plots of the filtered surface data were then prepared as a means of measuring image spatial similarity (as the macro-texture scale pushes the limit of conventional differencing techniques adopted for identifying similarity and change in point cloud analysis [56]).

3. Results and discussion

Nyquist values are given in Table 2. The 3D Smart Laser Profile Sensor minimum Nyquist wavelengths mean that the technique is unable to measure a small part of the lower range of macrotecture wavelengths between 0.5 and 1 mm. The SfM and TLS Nyquist wavelengths mean the techniques can measure the full range of macrotecture wavelengths and have the potential to also measure some part of microtexture below 0.5 mm, this capability should be explored as part of a further research study. The Nyquist wavelengths vary between samples, possibly because the techniques are sensitive to pavement surface albedo, environmental conditions, and edge effects. Given technique sensitivity, oversampling to ensure a sufficiently fine Nyquist wavelength is beneficial and in this regard adopting a higher resolution technique such as TLS is advantageous. The Nyquist wavelength for a TLS, will increase with distance from the laser source, because of the elongation of the beam, as the angle of incidence with a surface increases. Therefore, the optimal location to acquire TLS data with an ‘off-the-shelf scanner’, is within a narrow cone of incidence directly in line with the laser source, with data captured using an inverted head tripod set-up.

Surface height plots for each surface scanning technique are illustrated in Fig. 5. For the DBM greater similarity is evident between Fig. 5(a) and (b) as the 3D Smart Laser Profile Sensor and SfM techniques have similar resolution. The higher resolution of the TLS is evident in the finer granularity of plot Fig. 5(c). All the techniques are able to capture the voids between aggregates (e.g. i) and aggregate features (e.g. ii) on the DBM surface at the same locations. Equally, for the HRA surface there is greater similarity



Fig. 4. Field site: The field site was located adjacent to St James Church on Northumberland Road, Newcastle Upon Tyne, UK Grid Reference NZ 251 12 64814. (a) Conventional photograph of the field site. (b) Point cloud panorama of the site captured using the Faro Focus 3D X Series phased-based laser scanner. The three surfacing materials studied are (i) surface dressing, (ii) dense bitumen macadam, and (iii) hot rolled asphalt.

Table 2

Unfiltered and filtered results – point density, Nyquist length and areal surface texture parameters for the surfaces. The parameters are obtained from the raw point cloud data captured using the Faro Focus 3D X Series Phased-Based Laser Scanner, Structure from Motion and LMI Technologies Gocator 2350 Smart Laser Profile Sensor. Unfiltered results (top of table) demonstrate closer agreement between the Smart Laser Profile Sensor and Structure from Motion for S_q , and the linked parameters S_p and S_v (shown in bold). The spatial areal functions S_{pd} and S_{pc} representing the density and curvature of peak, (shown by previous researchers to have a positive correlation with skid resistance), are dissimilar and being sensitive to resolution, increase in magnitude with point density. The filtered results (bottom of table in grey) demonstrate increased agreement between S_{pd} and S_{pc} for the techniques, but the Smart Laser Profile Sensor and Structure from Motion techniques experience magnification of vertical measurements S_q , S_p and S_v in comparison to the unfiltered data.

	Parameter		Point Density (mm ⁻²)	Nyquist Wavelength (mm)	S_q (mm)	S_{sk}	S_p (mm)	S_v (mm)	S_{pd} (mm ⁻²)	S_{pc} (mm ⁻¹)
Unfiltered	Dense bitumen macadam	Smart sensor	0.97	$x = 1.02$ $y = 1.02$	0.951	-0.321	2.21	3.37	0.00354	0.1360
		SfM	35.80	$x = 0.167$ $y = 0.167$	0.949	-0.711	1.80	3.91	0.01110	0.7720
		TLS	83.59	$x = 0.091$ $y = 0.131$	1.090	-0.124	4.99	5.25	0.14100	27.8000
	Hot rolled asphalt	Smart sensor	4.19	$x = 0.489$ $y = 0.489$	1.280	-1.040	2.93	5.75	0.00185	0.2020
		SfM	26.47	$x = 0.184$ $y = 0.206$	1.370	-0.901	3.13	5.76	0.00273	0.6550
		TLS	163.84	$x = 0.073$ $y = 0.083$	1.560	-0.215	6.18	6.37	0.25000	76.8000
	Surface dressing	Smart sensor	3.39	$x = 0.547$ $y = 0.539$	0.544	-0.680	1.58	3.19	0.01110	0.4000
		SfM	31.19	$x = 0.145$ $y = 0.222$	0.557	-0.743	1.76	2.80	0.01140	0.5670
		TLS	63.27	$x = 0.142$ $y = 0.111$	0.938	-0.267	3.89	4.49	0.14000	17.9000
Filtered	Dense bitumen macadam	Smart sensor	0.66	$x = 1.23$ $y = 1.23$	3.940	-0.565	9.78	15.30	0.00166	0.3480
		SfM	24.37	$x = 0.202$ $y = 0.204$	3.660	-0.947	9.30	16.50	0.00253	0.3610
		TLS	55.67	$x = 0.120$ $y = 0.150$	0.738	-0.654	2.24	2.89	0.00225	0.0748
	Hot rolled asphalt	Smart sensor	3.74	$x = 0.519$ $y = 0.515$	12.600	-0.972	30.30	56.30	0.00223	2.4100
		SfM	23.95	$x = 0.194$ $y = 0.215$	13.300	-0.937	30.10	57.50	0.01640	17.4000
		TLS	148.19	$x = 0.078$ $y = 0.087$	3.200	-0.233	7.45	9.38	0.01970	5.0900
	Surface dressing	Smart sensor	2.31	$x = 0.664$ $y = 0.652$	2.000	-0.801	4.91	12.60	0.00196	0.2070
		SfM	20.61	$x = 0.194$ $y = 0.250$	2.390	-0.947	5.98	13.50	0.00240	0.2740
		TLS	42.63	$x = 0.165$ $y = 0.142$	0.607	-0.741	1.50	2.75	0.00250	0.7190

between Fig. 5(e) and (f), the data captured with the 3D Smart Laser Profile Sensor and SfM techniques. The higher resolution of the TLS is evident again in the finer granularity of the edges of the red chipping aggregate (Fig. 5g). Finally, although the SD aggregate chippings are the smallest for the three surfaces, all the techniques have still collectively identified areas of void between aggregates in blue Fig. 5(j)–(l) (e.g. vi) and areas of elevated macrotexture in orange located to the right and left edge of each plot. Again there is greater similarity between Fig. 5(j) and (k), the data capture with the 3D Smart Laser Profile Sensor and SfM technique. The higher resolution of the TLS is evident in the finer granularity of plot (l). The degree of similarity between the techniques has been characterised using areal parameters and 2D correlation analysis discussed in Section 3.1 and 3.2 respectively.

3.1. Unfiltered areal parameters

The areal parameters derived for each technique are given in Table 2. S_q is spatially equivalent to the mean profile depth that is used at present to evaluate macrotexture. Table 2 shows that S_q for the 3D Smart Laser Profile Sensor and SfM are within 0.002 mm agreement for the DBM, 0.013 mm for the SD and 0.09 mm for the HRA. This presents the 3D Smart Laser Profile Sensor and SfM, as an alternative method to capture texture depth. The TLS obtained results for S_q are very different, with differences in

comparison with the 3D Smart Laser Profile Sensor value ranging from 0.139 mm to 0.394 mm; the largest value being obtained for the SD surface. The value for S_p and S_v , the maximum peak and pit heights, demonstrate greater agreement between the SfM and 3D Smart Laser Profile Sensor results, than the TLS technique. The variance in TLS derived parameters is because of the higher resolution nature of the data. Values for S_{pd} and S_{pc} , which have previously been shown to have positive correlations with skid resistance [34], are typically different by an order of magnitude for all the techniques and surfaces considered. The variability of S_{pd} and S_{pc} suggests the parameters are also sensitive to resolution and limits the potential to adopt unfiltered data in ‘universal’ across technique parametric comparison studies with friction. For S_{sk} , the parameter defining skewness (thus indicating whether texture is positive or negative), all three unfiltered techniques were able to identify the positive texture of the surfaces. The skewness is sensitive to the spatial sampling resolution of the technique, with closer agreement demonstrated between the SfM and 3D Smart Sensor technique.

3.2. 2D correlation analysis

Areal parameters only characterise discrete functions of surface roughness. Therefore, 2D cross-correlation analysis to measure x-y and z plane similarity between images was completed. Perfect cor-

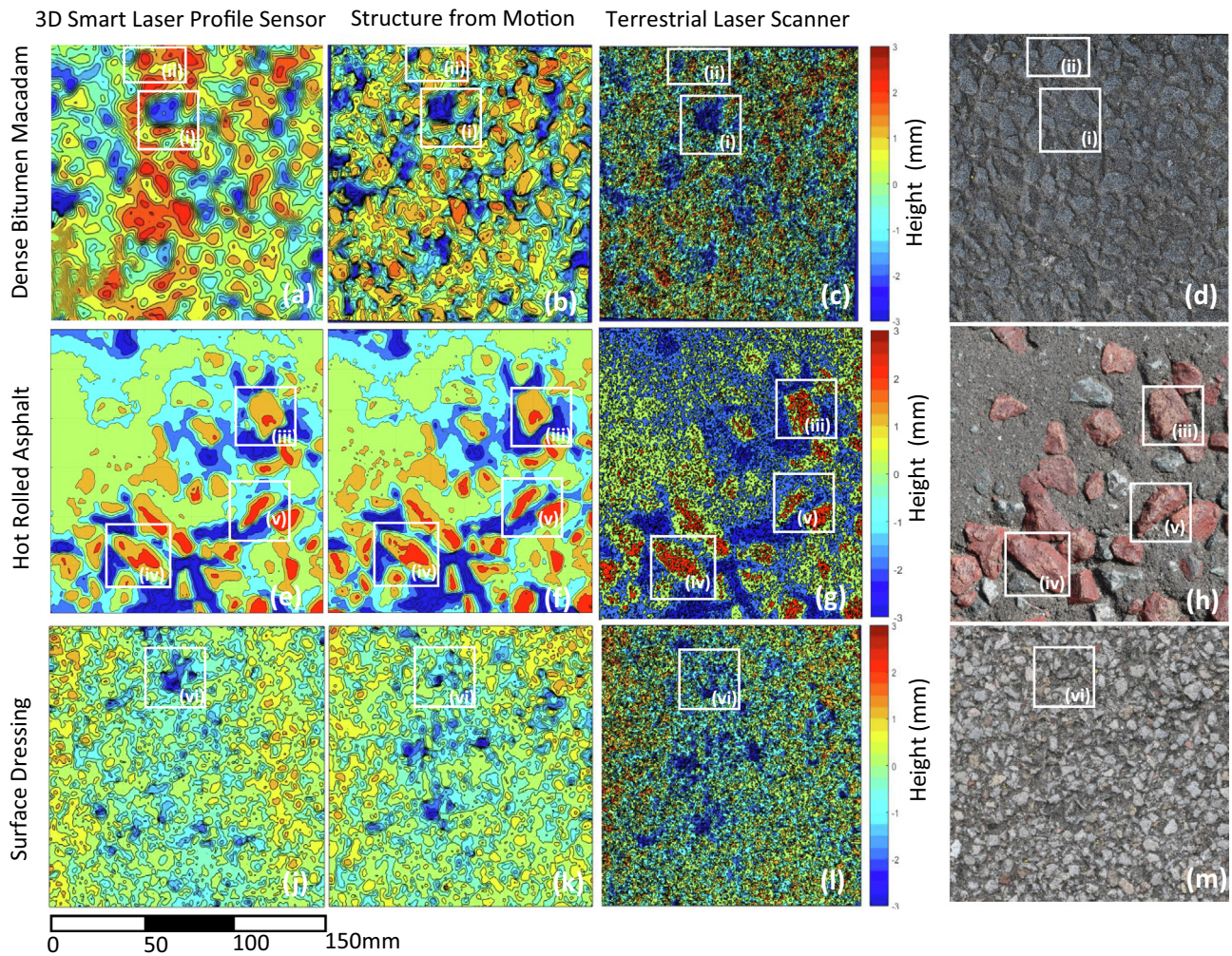


Fig. 5. Surface height plots derived from the unfiltered point cloud data for a 150 mm × 150 mm sample area of each surfacing material. (a) Dense Bitumen Macadam captured with 3D Smart Laser Profile Sensor (b) Dense Bitumen Macadam captured with Structure from Motion (c) Dense Bitumen Macadam capture with the Terrestrial Laser Scanner (d) Digital image of the Dense Bitumen Macadam surface. Greater similarity is evident between (a) and (b) as the 3D Smart Laser Profile Sensor and Structure from Motion techniques have similar resolution. The higher resolution of the Terrestrial Laser Scanner is evident in the finer granularity of plot (c). All the techniques are able to captured voids between aggregate (e.g. i) and aggregate features (e.g. ii) on the Dense Bitumen Macadam surface at the same locations. (e) Hot Rolled Asphalt captured with the 3D Smart Laser Profile Sensor (f) Hot Rolled Asphalt captured with Structure from Motion (g) Hot Rolled Asphalt captured with the Terrestrial Laser Scanner (h) Digital image of the Hot Rolled Asphalt surface. All three techniques have clearly captured the red aggregate chippings of the Hot Rolled Asphalt (e.g. iii to v). There is greater similarity between (e) and (f), the data captured with the 3D Smart Laser Profile Sensor and Structure from Motion techniques. The higher resolution of the Terrestrial Laser Scanner is evident in the finer granularity of the edges of the aggregate. (j) Surface Dressing captured with the 3D Smart Laser Profile Sensor (k) Surface Dressing captured with Structure from Motion (l) Surface Dressing Capture with the Terrestrial Laser Scanner. (m) Digital image of the Surface Dressing surface. There is greater similarity between (j) and (k), the data capture with the 3D Smart Laser Profile Sensor and Structure from Motion technique. The higher resolution of the Terrestrial Laser Scanner is evident in the finer granularity of plot (l). The Surfacing Dressing aggregate chippings are the smallest of the three surfaces, but the techniques have still collectively identified areas of void between aggregates in blue (e.g. vi) and areas of elevated macrotexture in orange located to the right and left edge of each plot.

relation is characterised by a strong central peak with a value of 1. The normalised 2D cross-correlation plots are shown in Fig. 6. For the DBM surface a central peak is evident of 0.4492 and 0.3515 for similarity between the 3D Smart Laser Profile Sensor and SfM, and 3D Smart Laser Profile Sensor and TLS respectively (Fig. 6(a) and (d)); defining positive correlation and symmetry (or lack of shift) between the wavelength frequencies. To the left of the central peak there is a dominating positive feature on both plots, depicted as the yellow to red zone (e.g., Fig. 6(a)–(i)), representing an area of higher macrotexture departure from the surface. For the SD surface, no central peak is evident with elongated bands of positive and negative agreement being visible (Fig. 6cii and ciii) for similarity between both the 3D Smart Laser Profile Sensor and SfM, and 3D Smart Laser Profile Sensor and TLS. The bands arise as the macrotexture of the SD surface is dominated by a repeating texture feature.

Overall, the best correlation is achieved between the 3D Smart Laser Profile Sensor and SfM measurement technique for the HRA surface Fig. 6(b). The plot has a clear strong centralised peak of 0.729, demonstrating an alignment or lack of lateral shift between the wavelength frequencies of the two techniques. The rest of the plot is generally blue indicating a general lack of secondary dominating features on the surface. This can be attributed to the parity of resolution between two techniques and the larger wavelength features of the HRA surface. The 2D cross-correlations affirm the areal parameter results with greater agreement between the unfiltered 3D Smart Laser Profile Sensor and SfM surface measurements. The 2D cross-correlation plots comparing similarity between the 3D Smart Laser Profile Sensor and TLS demonstrate less agreement. The normalised cross-correlation peaks are either not present or where present are lower being 0.3515 for the DBM (Fig. 6(d)). This confirms the influence of the higher resolu-

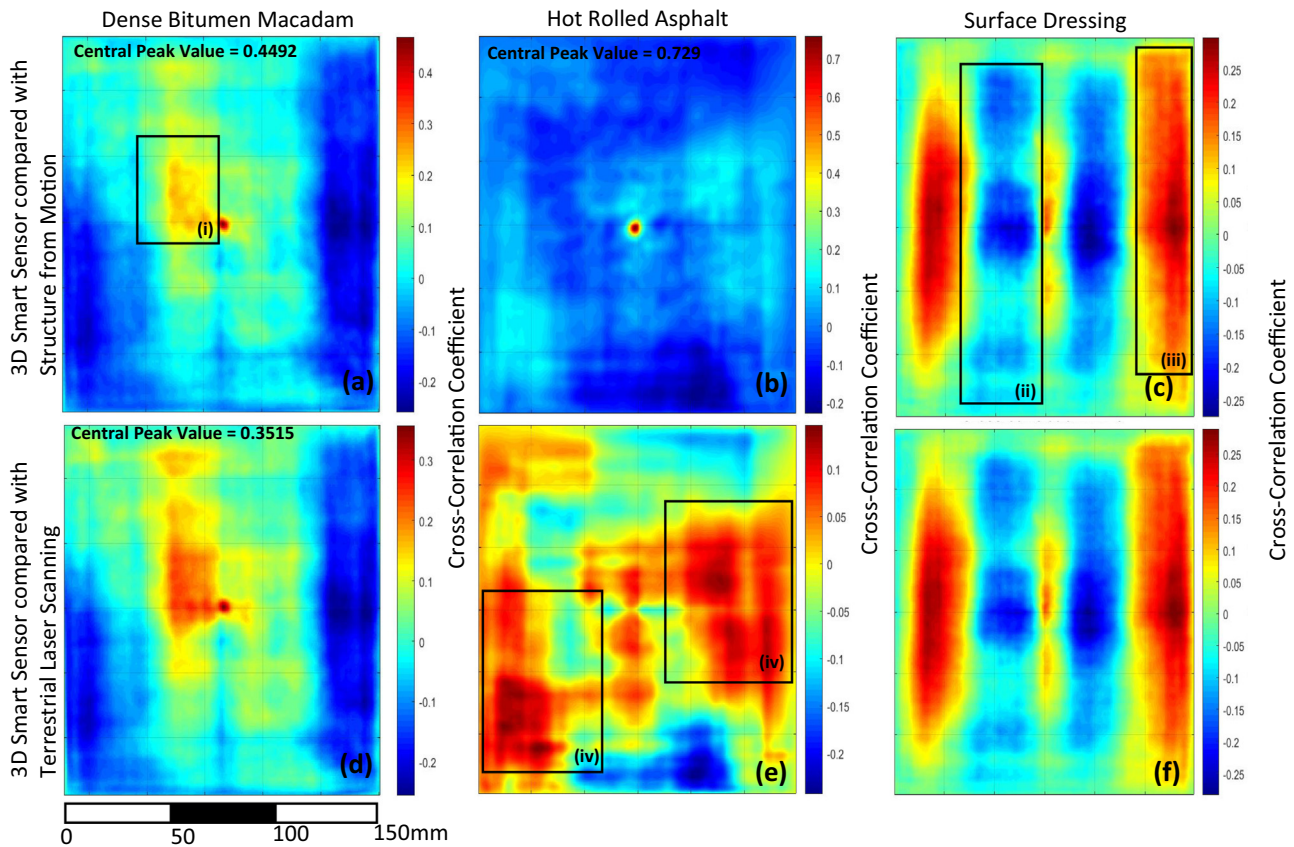


Fig. 6. 150 mm \times 150 mm 2D normalised cross-correlation plots for the unfiltered point cloud data. (a) 2D crosscorrelation plot, defining the similarity between the point cloud data obtain from the 3D Smart Sensor and Structure from Motion, for the Dense Bitumen Macadam surface. The plot has a clear strong centralised peak of 0.4492, demonstrating an alignment or lack of lateral shift between the wavelength frequencies of the two techniques. On the sidelobes there is a dominating positive feature, depicted as the yellow to red zone (i), representing an area of elevated macrotexture (b) 2D cross-correlation plot defining the similarity between the point cloud data obtain from the 3D Smart Sensor and Structure from Motion for the Hot Rolled Asphalt surface. The plot has a clear strong centralised peak of 0.729, demonstrating an alignment or lack of lateral shift between the wavelength frequencies of the two techniques. The sidelobes of the plot are generally blue indicating a general lack of secondary dominating features on the surface. (c) 2D cross-correlation plot defining the similarity between the point cloud data obtain from the 3D Smart Sensor and Structure from Motion for the Surface Dressing. No central peak is evident with instead elongated bands of positive and negative agreement being visible (ii and iii). The bands arise as the macrotexture of the SD surface is dominated by a repeating feature of bands of increased macrotexture height. (d) 2D crosscorrelation plot defining the similarity between the point cloud data obtain from the 3D Smart Sensor and the Terrestrial Laser Scanner for the Dense Bitumen Macadam surface. The plot is similar to (a) having a centralised peak of 0.3515 and a second dominating positive feature on the side lobes. (e) 2D cross-correlation plot defining the similarity between the point cloud data obtain from the 3D Smart Sensor and the Terrestrial Laser Scanner for the Hot Rolled Asphalt surface. No central peak is evident with instead two zones of positive agreement are visible on the sidelobes mirrored about the diagonal (iv and v). These represent the elevated macrotexture of the clustered zones of red aggregate chippings. (f) 2D cross-correlation plot defining the similarity between the point cloud data obtain from the 3D Smart Sensor and the Terrestrial Laser Scanner for the Surface Dressing. The plot is similar to (c).

tion shorter wavelengths within the unfiltered data, which cause the reduction in the normalised peak, and reduced agreement. After the application of a 0.1 wavenumber filter the heights of the normalised 2D cross- correlation peaks increase by 16.6–25% demonstrating stronger agreement between the 3D Smart Laser Profile Sensor and the other two techniques.

3.3. Filtered areal parameters

Surface height plots for each filtered surface scanning technique are illustrated in Fig. 7. For all three

surfaces after the application of a 0.1 mm^{-1} wavenumber filter there is greater visual similarity between all three techniques. The filter has reduced the resolution of the TLS data, removing the finer granularity, to reveal the macrotexture more clearly. Furthermore, post-filtering increased agreement was achieved for areal parameters Spd and Spc , previously shown to have a positive correlation with skid resistance. The filtered areal parameters are shown in Table 2. The filtered Spc (arithmetic mean peak curvature) values, related to the shape of the road aggregates, measured using the

3D Smart Laser Sensor and SfM are within 0.013 mm^{-1} for the DBM and 0.067 mm^{-1} for the SD. The filtered values of Spc for the HRA do not demonstrate agreement. The filtered Spd (peak density) values, related to the distribution of road aggregates upon a pavement surface, measured using the 3D Smart Laser Sensor and SfM are within 0.00087 mm^{-2} for the DBM, 0.01417 mm^{-2} for the HRA, and 0.00044 mm^{-2} respectively for the SD. The filtered Spd (peak density) values measured using the 3D Smart Laser Sensor and TLS are within 0.00059 mm^{-2} for the DBM, 0.01747 mm^{-2} for the HRA, and 0.00054 mm^{-2} for the SD. The filtered Spd values measured using the SfM and TLS are within 0.00028 mm^{-2} for the DBM, 0.0033 mm^{-2} for the HRA, and 0.0001 mm^{-2} for the SD. Although an increased agreement has been achieved for Spd and Spc , importantly for practical pavement characterisation of surface height departures, for the 3D Smart Laser Profile Sensor and SfM techniques this is at the expense of the accuracy of Sq , which experiences magnification at a range of four to ten times. Therefore, filtering improves spatial agreement, but at the cost of vertical measurement, a factor that should be considered by researchers seeking correlations between non-contact texture measurements

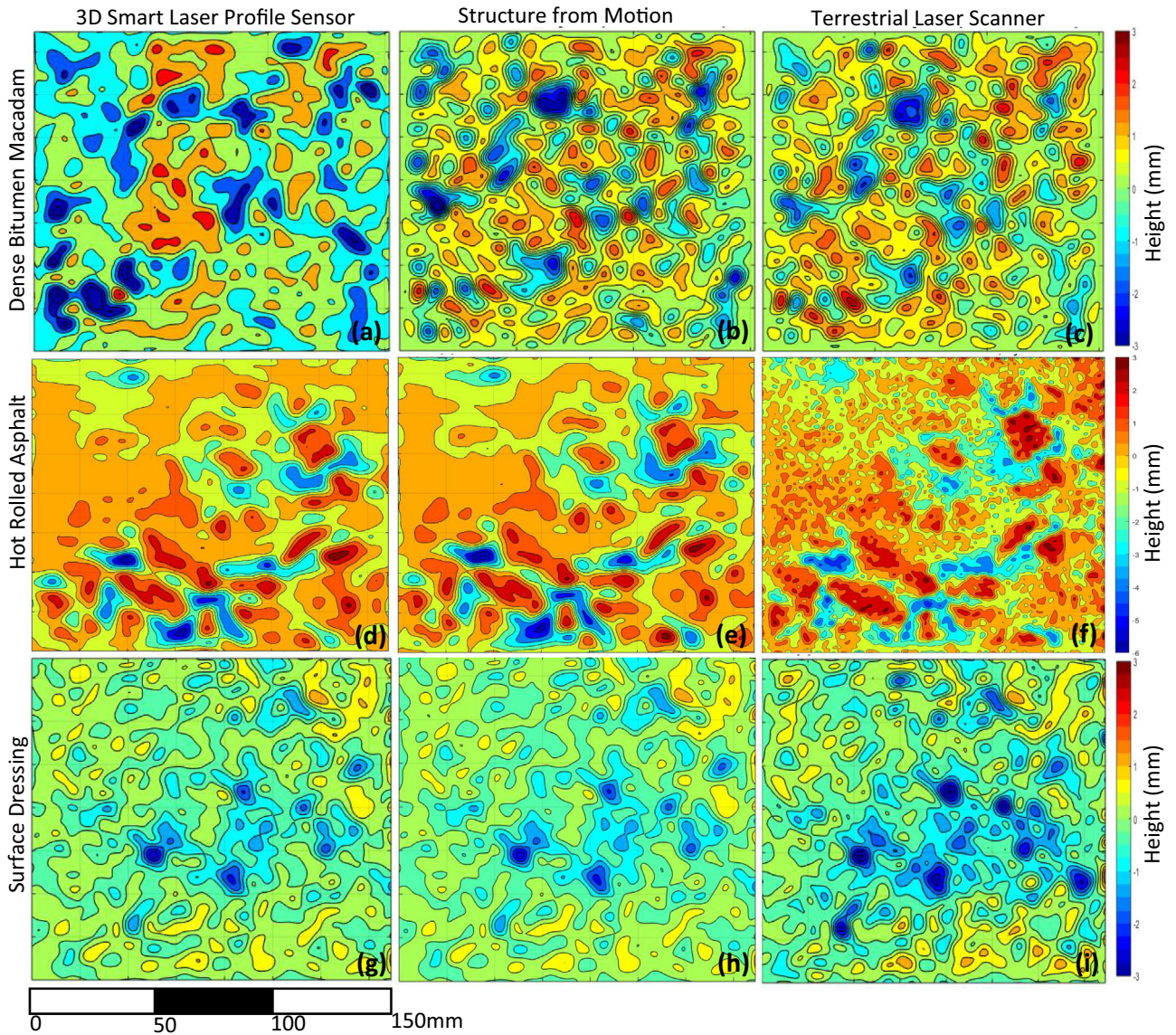


Fig. 7. Surface height plots derived from the 0.1 wavenumber filtered point cloud data for a 150 mm × 150 mm sample area of each surfacing material. (a) Dense Bitumen Macadam captured with 3D Smart Laser Profile Sensor (b) Dense Bitumen Macadam captured with Structure from Motion (c) Dense Bitumen Macadam capture with the Terrestrial Laser Scanner. After the application of a 0.1 wavenumber filter there is greater visual similarity between the Structure from Motion and Terrestrial Laser Scanner data. The filter has reduced the resolution of the Terrestrial Laser Scanner data, removing the finer granularity, to reveal the macrotexture more clearly. (d) Hot Rolled Asphalt captured with the 3D Smart Laser Profile Sensor (e) Hot Rolled Asphalt captured with Structure from Motion (f) Hot Rolled Asphalt captured with the Terrestrial Laser Scanner. After the application of a 0.1 wavenumber filter there is greater visual similarity between all three techniques. The filter has reduced the resolution of the Terrestrial Laser Scanner data, removing some of the finer granularity, to reveal the macrotexture more clearly. (g) Surface Dressing captured with the 3D Smart Laser Profile Sensor (h) Surface Dressing captured with Structure from Motion (i) Surface Dressing Capture with the Terrestrial Laser Scanner. After the application of a 0.1 wavenumber filter there is greater visual similarity between all three techniques. The filter has reduced the resolution of the Terrestrial Laser Scanner data, removing the finer granularity, to reveal the macrotexture more clearly. All techniques have generally identified the same areas as voids between aggregates in blue, and areas of elevated texture in orange.

and skid resistance. Moreover, the filtered values of S_q obtained from the TLS whilst closer to the original unfiltered 3D Smart Laser Profile Sensor, demonstrate at best ten percent accuracy; being in 0.213 mm agreement for the DBM, 1.928 mm agreement for the HRA and 0.063 mm agreement for the SD. The TLS technique does offer the best balance between the vertical and spatial areal functions post-filtering, fundamentally because it enables oversampling of the surfaces, with correspondingly the shortest Nyquist wavelength. However, the improved resolution of the technique still does not lead to sufficiently accurate measurement of S_q , the vertical departure heights from a pavement surface. Greater technique resolution does not necessarily equate to sufficiently improved accuracy for some measurements.

3.4. Spectral analysis

The spectra in Fig. 8 illustrate the areal wavenumber characteristics of the three surface materials in the 'x' and 'y' plane [55]. As wavenumber is the reciprocal of wavelength, the plots serve to demonstrate differences in macrotexture characteristic between the surfaces. The spectra are sensitive both to the scale of the macrotexture and the technique of measurement. The TLS has the largest spectral cloud of the three techniques for all surfaces, illustrating that it is consistently the highest resolution technique. Considering the SfM spectral plots, it is clear that the HRA surface has the largest wavelength features represented by the brightest spectral cloud centre; whilst the DBM contains the smallest wave-

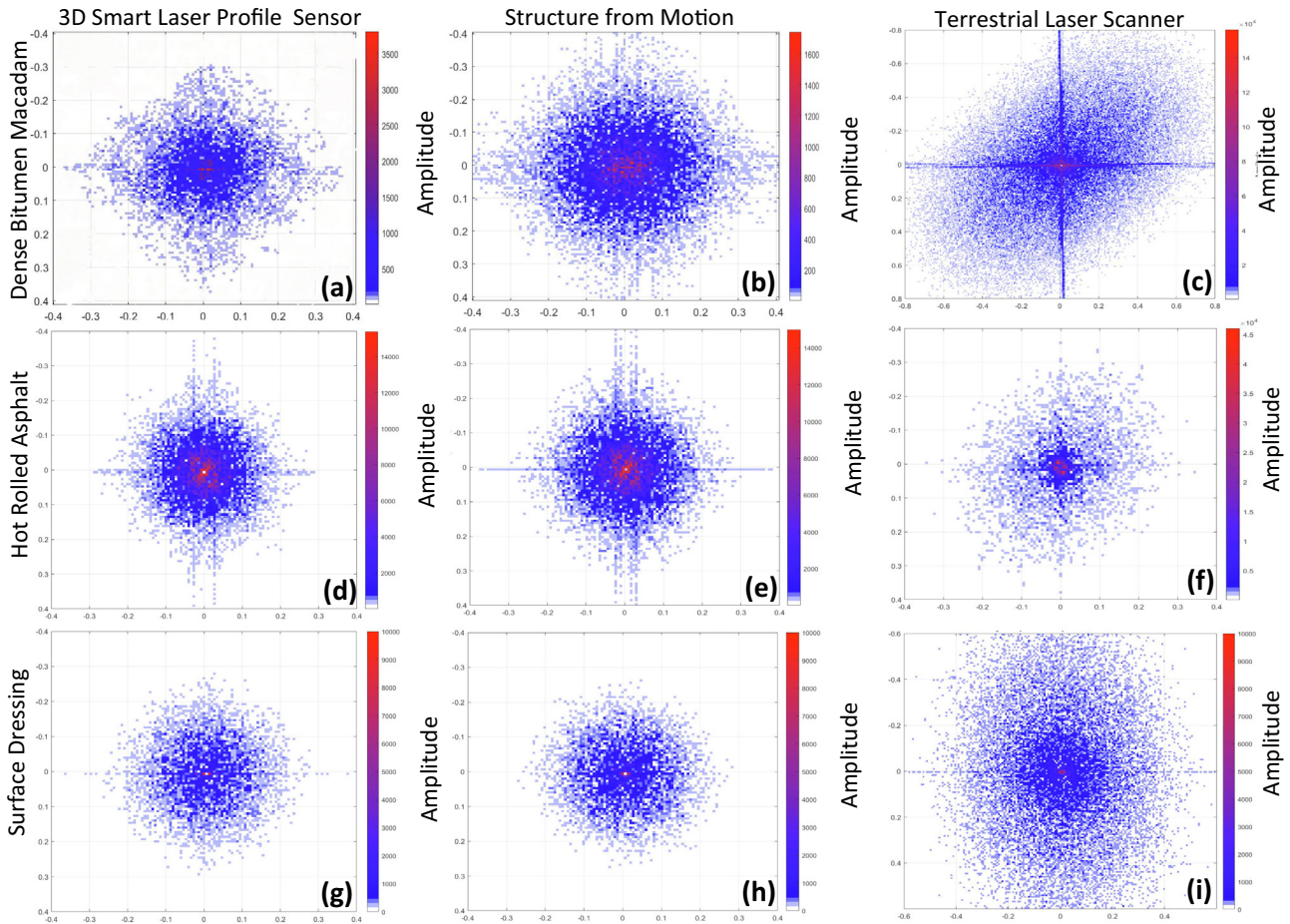


Fig. 8. 2D wavenumber (mm^{-1}) spectral analysis of the unfiltered point cloud data. (a) Wavenumber spectral analysis for the 3D Smart Laser Profile Sensor scan of the Dense Bitumen Macadam surface. (b) Wavenumber spectral analysis for the Structure from Motion scan of the Dense Bitumen Macadam surface. (c) Wavenumber spectral analysis for the Terrestrial Laser scan of the Dense Bitumen Macadam surface. (d) Wavenumber spectral analysis for the 3D Smart Laser Profile Sensor scan of the Hot Rolled Asphalt surface. (e) Wavenumber spectral analysis for the Structure for Motion scan of the Hot Rolled Asphalt surface. (f) Wavenumber spectral analysis for the 3D Terrestrial Laser scan of the Hot Rolled Asphalt surface. (g) Wavenumber spectral analysis for the 3D Smart Laser Profile Sensor scan of the Surface Dressing. (h) Wavenumber spectral analysis for the Structure from Motion scan of the Surface Dressing. (i) Wavenumber spectral analysis for Terrestrial Laser scan of the Surface Dressing.

length features represented by the largest cloud. As a high pass filter was not applied to the cloud data, the larger wavelengths in the centre of the spectral plots represent the unevenness of the surfaces. The spectra reveal that for the SfM technique that for the HRA the wavelengths features are typically 4 mm or larger; the SD 3.5 mm or larger and DBM 2.6 mm or larger. Finally, greater similarity is generally evident between the unfiltered spectra for the SfM and 3D Smart Laser Profile Sensor, as the techniques have similar resolution and accuracy.

3.5. Spatial variability

The spatial variability of S_q , S_{sk} , S_p , S_v , S_{pd} and S_{pc} for seventy-two $150 \text{ mm} \times 150 \text{ mm}$ samples and eighteen $300 \text{ mm} \times 300 \text{ mm}$ samples captured using SfM were considered for a $1.8 \text{ m} \times 0.9 \text{ m}$ area of HRA in Figs. 9 and 10.

The computed parameters (S_q , S_{sk} , S_p , S_v , S_{pd} and S_{pc}) for each individual sample, were divided into a percentage of the overall maximum for each considered areal parameter, with the discrete colour contrasts representing 20%. Thereby each colour represents a 20th percentile in the overall maximum parameter value, and thus illustrates the variability of the parameters across the $1.8 \text{ m} \times 0.9 \text{ m}$ HRA surface. The $150 \text{ mm} \times 150 \text{ mm}$ sample size for S_p , maximum peak height, reflects the distribution of red aggregate chippings across the HRA surface. Lower peaks are encoun-

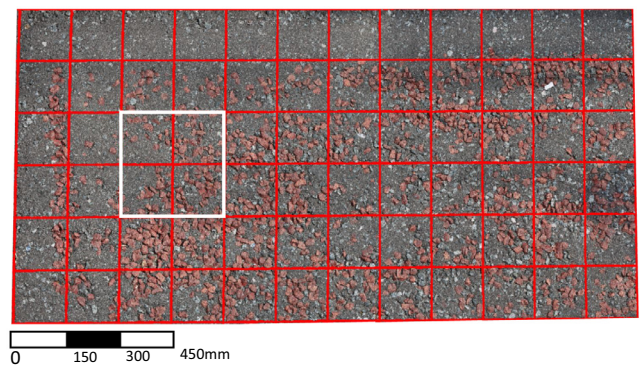


Fig. 9. Digital image of the $1.8 \text{ m} \times 0.9 \text{ m}$ area of Hot Rolled Asphalt considered in the spatial variance study. The parameters S_q , S_{sk} , S_p , S_v , S_{pd} , and S_{pc} are computed from raw point cloud data captured using Structure from Motion for the $150 \text{ mm} \times 150 \text{ mm}$ samples delineated by the red lines. The parameters parameters S_q , S_{sk} , S_p , S_v , S_{pd} , and S_{pc} were recomputed on the same point cloud data for the $300 \text{ mm} \times 300 \text{ mm}$ samples. The $300 \text{ mm} \times 300 \text{ mm}$ directly overlapped the original $150 \text{ mm} \times 150 \text{ mm}$ samples (as illustrated by the white square).

tered near the top edge of the sample, where the surface is predominantly bituminous binder. Some discrete squares of increased peak height are shown in dark green, representing the

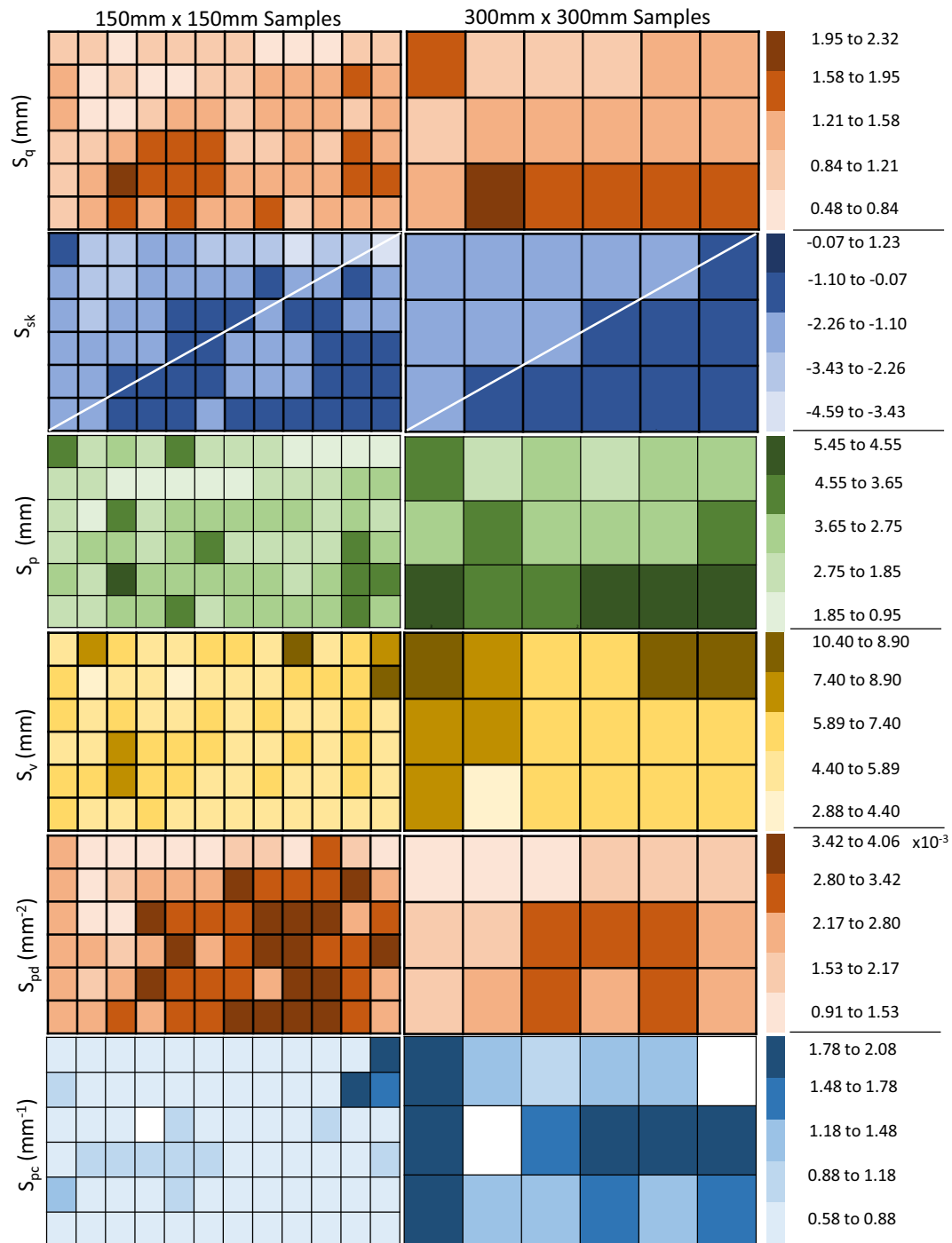


Fig. 10. Spatial variance of S_q , S_{sk} , S_p , S_v , S_{pd} , S_{pc} over a $1.8 \text{ m} \times 0.9 \text{ m}$ area of Hot Rolled Asphalt surfacing for $150 \text{ mm} \times 150 \text{ mm}$ and $300 \text{ mm} \times 300 \text{ mm}$ samples, data captured with Structure from Motion. The computed parameters for each individual sample, were divided into a percentage of the overall maximum for each areal parameter. Each discrete colour contrasts representing a 20 percentile difference in parameter values. The colour tone difference demonstrates the variability of the parameters across the $1.8 \text{ m} \times 0.9 \text{ m}$ hot rolled asphalt surface.

higher texture height of isolated red chippings. Principally, the peak height values S_p are within the percentile range of 1.85 mm to 3.65 mm. The $150 \text{ mm} \times 150 \text{ mm}$ sample size for S_v , maximum pit height, demonstrated limited variability between separate sample areas, with 87.5% of the HRA surface being within 4.4–7.4 mm. This consistency most likely reflects the method of laying HRA, with the precoated red aggregate chippings being scattered across the surface of the previously laid asphalt binder and rolled into the surface at a constant pressure, resulting in more consistent pit

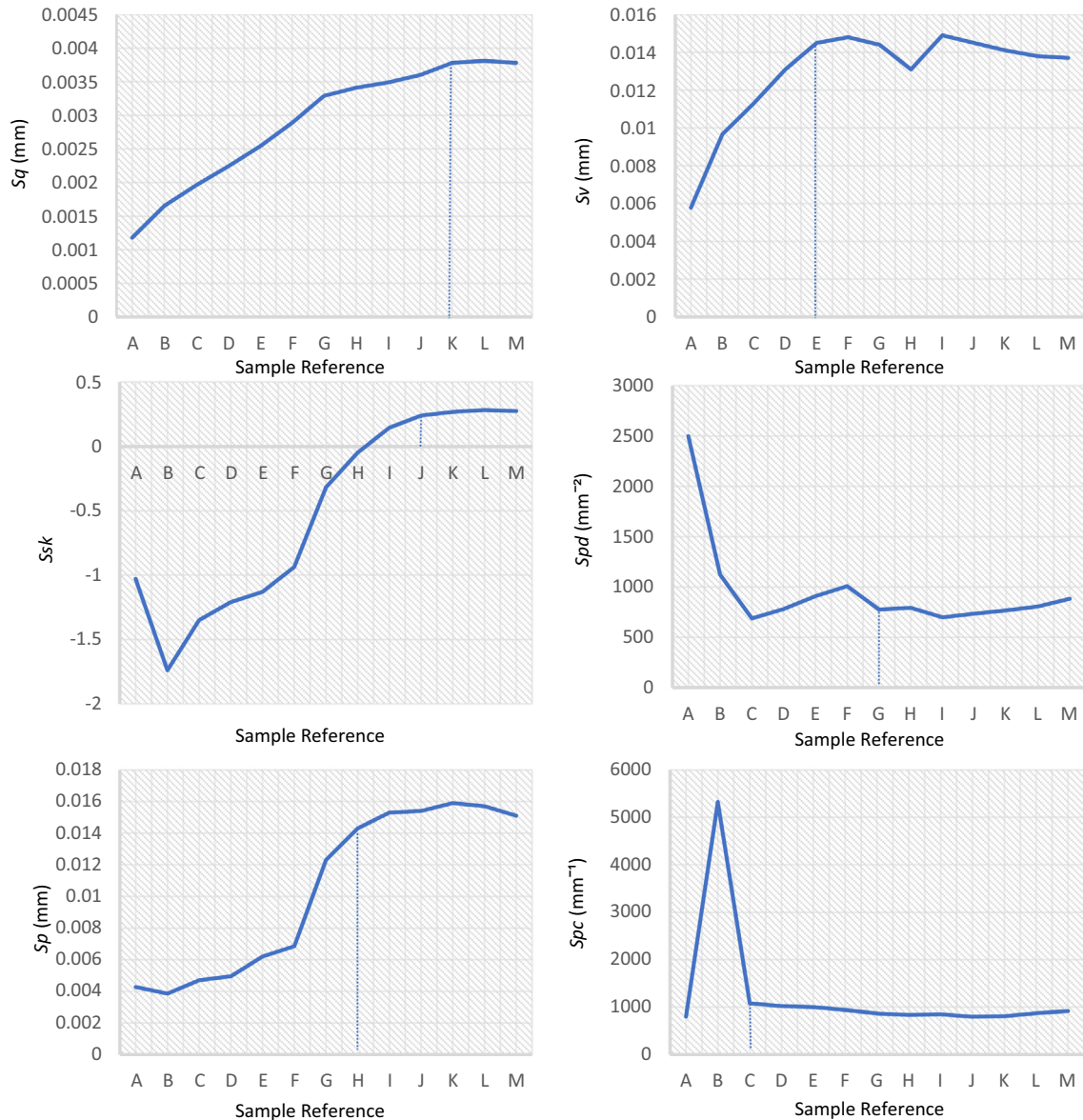
heights. For vertical macrotexture characterisation parameters, such as S_v , S_p and S_q spatially equivalent to the mean profile depth used at present to evaluate macrotexture, there is some similarity between the location of darker colour contrast for both the $150 \text{ mm} \times 150 \text{ mm}$ and $300 \text{ mm} \times 300 \text{ mm}$ sample sizes.

There is a lack of parity between the surface characterised using the $150 \text{ mm} \times 150 \text{ mm}$ sample and the $300 \text{ mm} \times 300 \text{ mm}$ sample for S_{pd} ; with an increase in sample size appearing to 'smooth' the density of peaks removing altogether the highest percentile range

$3.42 \times 10^{-3} \text{ mm}^{-2}$ to $4.06 \times 10^{-3} \text{ mm}^{-2}$ from the $300 \text{ mm} \times 300 \text{ mm}$ plot. The $150 \text{ mm} \times 150 \text{ mm}$ samples reflect the distribution of red chippings across the surface, with the lower peak densities recorded near the top and edge of the HRA surface where there is predominantly bituminous binder present. The *Spd* parameter also demonstrates the greatest variability between different $150 \text{ mm} \times 150 \text{ mm}$ samples. *Spd* has previously been shown as being important to skid resistance, with positive correlation achieved with friction measurements. However, the variability of *Spd* values, means picking a representative $150 \text{ mm} \times 150 \text{ mm}$ sample to characterise the whole surface to correlate with friction

is difficult. *Spd* represents the number of peaks in a unit area and is sensitive to sample size. Fig. 11 considered the influence of upscaling the sample size for areal parameters (*Sq*, *Ssk*, *Sp*, *Sv*, *Spd* and *Spc*) on the HRA surfacing capture using SfM with the point cloud extended to $1.05 \text{ m} \times 1.95 \text{ m}$. For *Spd* the optimum sample size for the HRA surface was found to be $1050 \text{ mm} \times 1050 \text{ mm}$. For the vertical macrotexture parameters, the optimum sample size was found to be $750 \text{ mm} \times 750 \text{ mm}$ for *Sv*, $1050 \text{ mm} \times 1200 \text{ mm}$ for *Sp*, and $1050 \text{ mm} \times 1650 \text{ mm}$ for *Sq*.

For *Spc* mean curvature of peaks, the optimum sample size was discovered to be $450 \text{ mm} \times 450 \text{ mm}$ for the HRA surface. *Spc* was



Sample Reference	Size (mm)	Sample Reference	Size (mm)
A	150 x 150	G	1050 x 1050
B	300 x 300	H	1050 x 1200
C	450 x 450	I	1050 x 1350
D	600 x 600	J	1050 x 1500
E	750 x 750	K	1050 x 1650
F	900 x 900		

Fig. 11. The influence of upscaling sample size on areal parameters *Sq*, *Ssk*, *Sp*, *Sv*, *Spd*, *Spc* for an area of Hot Rolled Asphalt surfacing captured using Structure from Motion. The optimum sample size for each parameter is indicated on each graph with a dotted line, and occurs where values converge to a stable value.

found to have the smallest sample size of all the parameters considered perhaps reflecting its general lack of heterogeneity. The 150 mm × 150 mm sample size demonstrating the least variability across the HRA surface of any of the areal parameters considered by the study; with 80% of the samples falling within the 20% range 0.58 mm⁻¹–0.88 mm⁻¹.

Whilst *Sq*, *Sp*, and *Sv* just capture the overall height and depth of peak and pit surface departures, *Ssk* gives the location (or skewness) above and below the mean plane; consequently, providing an indication of the distribution of texture available to contribute to skid resistance. For *Ssk*, both the 150 mm × 150 mm and 300 mm × 300 mm sized samples confirm that the HRA has positive texture. The split of the contrasting light and dark blue squares for *Ssk*, is similar for each sample size, with the predominant number of darker squares below the white diagonal line bisecting the 1.8 m × 0.9 m area (refer to Fig. 10). However, the location of the mean plane was determined to be sensitive to sample size, with the value of *Ssk* varying. A sample size of 1050 mm × 1200 mm of smaller was found in the upscaling analysis to have a negative texture confirming a positive texture, but above this size *Ssk* was shown to have a positive value indicating a skew to negative texture. The change in *Ssk* can be attributed to the influence of the variability of peak height with changing sample area, on the location of the mean plane. Overall reviewing individual areal parameters typically used to characterise friction (*Sp*, *Sv*, *Spd* and *Spc*) optimal sample size, suggests that a suitable sample size of 1050 mm × 1200 mm is appropriate to characterise HRA; this being established from the maximum size of the individual parameters

Further research should be conducted to explore the efficiency of sample sizes for areal parameters for different pavement textures. As contact friction devices are known to be susceptible to seasonal variation and machine operating conditions such as load, speed slip ratio and the composition of rubber, using reliable non-contact areal parameter data to be able to analytically model a relationship with friction is desirable. Moreover, higher resolution does not always equate to greater accuracy. It was found that whilst SfM photogrammetry successfully provides an alternative method to the 3D Smart Laser Profile Sensor to capture vertical pavement measurement *Sv*, *Sp* and *Sq* for mean profile depth estimation and correlation with friction, the higher resolution TLS data contained significant inaccuracies. Furthermore, the values of *Spd* and *Spc*, which together define the shape and distribution of pavement aggregates and have previously been proven to have positive correlation with friction [34], are sensitive to resolution, incurring order of magnitude differences. A 2D low pass wavenumber filter achieved improved agreement with the 3D smart profiler for *Spd* and *Spc* parameters. Optimising such filters consistently across a range of non-contact techniques is needed to achieve a 'universal' correlation between these parameters and to model relationships with skid resistance. Further, as the application of such a filter has the potential to impact on vertical accuracy of measurement (*Sq*, *Sp*, and *Sv*) for some high resolution techniques, findings of this study indicate the filter should be applied only to the *Spd* and *Spc* spatial parameters.

4. Conclusions

In conclusion, the study has compared the measurement of macrotexture using three different techniques. The study makes a first contribution to the establishment of reliable standardised texture measurements using point cloud derived data to inform analytical prediction methods for tyre-pavement contact friction without the influences of seasonal variation, measuring devices and their operating conditions. Results from the analysis of the data lead to the following conclusions:

- Unfiltered close field SfM photogrammetry provides values of *Sp*, *Sv* and *Sq*, within an acceptable degree of tolerance to those obtained from the 3D Smart Laser Profile Sensor, so as SfM photogrammetry is an effective, readily scalable alternative method to capture mean profile depth for pavement evaluation.
- The parameters *Spc* and *Spd*, for which previous studies have established an important correlation with pavement friction, are sensitive to technique resolution and a 2D low pass wavenumber filter needs to be applied to obtain a 'universal' measurement for pavement friction assessment.
- A 2D zero-phase wavelength filter of 0.1 mm⁻¹ improves *Spd*, for the TLS and SfM techniques.
- The Nyquist wavelengths of TLS and SfM techniques mean they have the potential to measure microtexture wavelengths below 0.5 mm.
- TLS data are significantly improved for macrostructure surveys after 2D low pass wavenumber filtering.
- Where 150 mm × 150 mm industry sample sizes are used to determine parameters from point clouds data derived from non-contact techniques, these are not sufficient to correctly characterise functional areal parameters to describe the spatial variability of macrotexture upon a pavement. This study suggests a suitable sample size of 1050 mm × 1200 mm is appropriate to characterise HRA.

Declaration of Competing Interest

The authors declare that they have no known competing financial interests or personal relationships that could have appeared to influence the work reported in this paper.

References

- [1] Design Manual for Roads and Bridges, HD28/15: Skid Resistance. Norwich: The Stationary Office, Office of Public Sector Information. Volume 7, Section 3, Part 1, 2015. [Online] Available at: <http://www.standardsforhighways.co.uk/ha/standards/dmrb/vol7/section3/hd2815.pdf> (accessed 27.01.18).
- [2] D.F. Moore, *The Friction of Pneumatic Tyres*, Elsevier, New York, 1975.
- [3] M. Klüppel, G. Heinrich, Rubber friction on self affine road tracks, *Rubber Chem. Technol.* 73 (2001) 578–606, <https://doi.org/10.5254/1.3547607>.
- [4] B.N.J. Persson, *Sliding Friction: Physical Principles and Applications*, Springer-Verlag, Berlin, 2001.
- [5] M. Kane, V. Edmondson, Modelling the bitumen scour effect: enhancement of a dynamic friction model to predict the skid resistance of rubber upon asphalt surfaces subject to wear by traffic polishing, *Wear* 400–401 (2018) 100–110, <https://doi.org/10.1016/j.wear.2017.12.013>.
- [6] M.T. Do, V. Cerezo, Road surface texture and skid resistance, *Surf. Topogr. Metrol. Prop.* 3 (2015) 1–16, <https://doi.org/10.1088/2051-672X/3/4/043001>.
- [7] J.W. Hall, K.L. Smith, L. Titus-Glover, J.C. Wambold, T.J. Yager, Z. Rado, *Guide for Pavement Friction: Final Report for National Cooperative Highway Research Program (NCHRP) Project 01-43*, Transport Research Board of the National Academies, Washington, D.C., 2009 (accessed 27.01.18).
- [8] PIARC, Report of the committee on surface characterisation, in: Permanent International Association of Road Congress (PIARC) XVIII World Road Congress, Brussels, 1987 [Online] Available at: <https://www.piarc.org/en/publications/Congress-Proceedings/Brussels-1987/technical-committee-report.htm> (accessed 27.01.18).
- [9] A. Dunford, Friction and the texture of aggregate particles used in the road surface course PhD thesis, University of Nottingham, UK, 2013. [Online] Available at: <http://eprints.nottingham.ac.uk/13412/> (accessed 27.01.2018).
- [10] A. Dunford, Road surfaces, in: R. Leach (Ed.), *The Characterisation of Areal Surface Texture*, Springer, Teddington, 2013, pp. 337–348. ISBN-13:978-3-642-36457-0.
- [11] G. Flintsch, E. De Leon, K. McGhee, I. Al-Qadi, Pavement surface macrotexture measurement and applications, *Trans. Res. Rec.* 1860 (2013), <https://doi.org/10.3141/1860-19>.
- [12] R.G. Roe, R. Sinhal, The polished stone value of aggregates and in service skidding resistance, TRL report 322, TRL, Crowthorne, UK, 1998 [Online] Available at: <https://trl.co.uk/reports/TRL322> (accessed 27.01.18).
- [13] Z. Rado, M. Kane, An initial attempt to develop an empirical relation between texture and pavement friction using the HHT approach, *Wear* 309 (1–2) (2014) 233–246, <https://doi.org/10.1016/j.wear.2013.11.015>.
- [14] BS EN 13032-1:2010, Road and airfield surface characteristics – Test method. Part 1: Measurement of pavement surface macrotexture depth using

- volumetric patch techniques. British Standard Institute. London ISBN-13: 9780580685613.
- [15] British Standards Institute, BS EN 13036-4:2011: Road and Airfield Surface Characteristics of Slip/skid Resistance of a Surface: The Pendulum Test, British Standards Institute, London, 2011.
 - [16] British Standards Institute, BS7941-1: 2006 Method of Measuring the Skid Resistance of Pavement Surfaces Sideway-force coefficient routine investigation machine, British Standards Institute, London, 2006.
 - [17] British Standards Institute, BS7941-2:2000, Method of Measuring the Skid Resistance of Pavement Surfaces. Test Method for Measurement of Surface Skid Resistance Using the Grip Tester Braked Wheel Fixed Slip Device, British Standards Institute, London, 2000. ISBN-10: 0580332101.
 - [18] R.B. Kogbara, E.A. Masad, E. Kassem, A.T. Scarpas, K. Anupam, A state-of-the-art review of parameters influencing the measurement and modelling of skid resistance of asphalt pavements, *Construct. Build. Mater.* 114 (2016) 602–617, <https://doi.org/10.1016/j.conbuildmat.2016.04.002>.
 - [19] W. Bijsterveld, M.A. de Val, Towards quantification of seasonal variation in skid resistance measurement, *Road Mater. Pavement Des.* 17 (2) (2016) 477–486, <https://doi.org/10.1080/14680629.2015.1090909>.
 - [20] J.R. Hosking, G.C. Woodford, TTRL Report 738, Measurement of skidding resistance Part II. Factors effecting the slipperiness of a road surface. Crowthorne: Transport and Road Research Laboratory (1967) [Online] Available at: <https://trl.co.uk/reports/LR738> (accessed 27.01.18).
 - [21] M.A. Kahasawneh, R.Y. Laing, Temperature effects on the frictional properties of HMA at different polishing stages, *Jordan J. Civ. Eng.* 6 (1) (2012) 39–53.
 - [22] R.H. Smith, *Analysing Friction in the Design of Rubber Products and their Paired Surfaces*, CRC Press (Taylor and Francis Group), Boca Raton, Florida, 2008 ISBN-13:9780849381379.
 - [23] C. Plati, K. Georgouli, A. Loizos, Utilising the seasonal variations of skid resistance to plan preventative maintenance, in: M. Losa, T. Pagagiannakis (Eds.), *Sustainability, Eco-Efficiency and Conservation in Transportation Infrastructure Asset Management*, CRC Press (Taylor and Francis Group), Boca Raton, Florida, 2014, pp. 509–518. ISBN-13:9781138001473.
 - [24] P.D. Sanders, S. McRobbie, J. Gopaladas, H.E. Viner, Report Number PPR771 Development of a Reference Surface for the Assessment of Pavement Skid Resistance Measurement Devices, Transport Research Laboratory, Crowthorne, 2015 (accessed 27.01.18).
 - [25] A. Dunford, PPR315 Measuring skid resistance without contact, Transport Research Laboratories, Crowthorne, 2008 (accessed 27.01.18).
 - [26] M. Kane, M.T. Do, V. Cerezo, Z. Rado, C. Khelifi, Contribution to pavement friction modelling an introduction to the wetting effect, *Int. J. Pavement Eng.* (2017) p1–p12.
 - [27] M. Kane, V. Cerezo, A contribution to tire/road friction modelling: From a simplified dynamic friction contact model to a 'Dynamic Friction Tester' model, *Wear* 342–343 (2015) 163–171.
 - [28] A. Ueckermann, D. Wang, M. Oeser, B. Steinauer, Calculation of skid resistance from texture measurements, *J. Traffic Transport. Eng.* 2 (1) (2015) 3–16, <https://doi.org/10.1016/j.jtte.2015.01.001> (English Edition).
 - [29] X. Zhang, T. Liu, C. Liu, Z. Chen, Research on skid resistance of asphalt pavement based on three-dimensional laser-scanning technology and pressure-sensitive film, *Construct. Build. Mater.* 69 (2014) 49–59, <https://doi.org/10.1016/j.conbuildmat.2014.07.015>.
 - [30] V.M.C. Araujo, I.S. Bessa, V.T.F. Castelo Branco, Measuring skid resistance of hot mix asphalt using the aggregate image measurement system (AIMS), *Construct. Build. Mater.* 98 (2015) 476–481, <https://doi.org/10.1016/j.conbuildmat.2015.08.117>.
 - [31] B. Prowell, D. Hanson, Evaluation of circular texture meter for measuring surface texture of pavements, transport research record, *J. Transport. Res. Board* (1929), <https://doi.org/10.3141/1929-11>.
 - [32] S. Li, S. Noureldin, K. Zhu, Y. Jaing, Pavement surface microtexture: testing characterisation and frictional interpretation, in: B. Choubane (Ed.), *Pavement Performance: Current Trends, Advance and Challenges*; ASTM STP 1555, American Society for Testing Materials (ASTM), West, Conshohocken, PA, 2012, pp. 59–76, <https://doi.org/10.1520/STP104426>.
 - [33] A. Shalaby, A. El Gendy, Digital Image Analysis: Current Practice of Pavement Texture Measurement, in 8th International Transportation Speciality Conference, Winnipeg, Manitoba, June 9th to 12th (2010) pp1313 to 1321 [Online] Available at: https://www.researchgate.net/publication/290284577_Digital_image_analysis_Current_practice_of_pavement_texture_measurement (accessed 27.01.18).
 - [34] R.B. Kogbara, E.A. Masad, D. Woodward, P. Millar, Relating surface texture parameters from close range photogrammetry, *Construct. Build. Mater.* 166 (2018) 227–240, <https://doi.org/10.1016/j.conbuildmat.2018.01.102>.
 - [35] M.N. Alamdarlo, S. Hasami, Optimization of the photometric stereo method for measuring pavement texture properties, *Measurement* 127 (2018) 406–413, <https://doi.org/10.1016/j.measurement.2018.05.109>.
 - [36] F.G. Pratico, A. Astolfi, A new and simplified approach to assess the pavement surface micro- and macrotexture, *Construct. Build. Mater.* 148 (2017) 476–483, <https://doi.org/10.1016/j.conbuildmat.2017.05.050>.
 - [37] L. Gao, M. Lui, Z. Wang, J. Xie, S. Jia, Correction of texture depth of porous asphalt pavement based on CT scanning technique, *Constr. Build. Mater.* 200 (2019) 514–520, <https://doi.org/10.1016/j.conbuildmat.2018.12.154>.
 - [38] W. Wang, X. Yan, H. Huang, X. Chu, M. Abdel-Aty, Design and verification of a laser based device for pavement macrotexture measurement, *Trans. Res. Part C* 19 (2011) p682–p694.
 - [39] D. Zhang, Q. Zou, H. Lin, X. Xu, L. He, R. Gui, Q. Li, Automatic pavement defect detection using 3D laser profiling technology, *Automat. Constr.* 96 (2018) 350–365, <https://doi.org/10.1016/j.autcon.2018.09.019>.
 - [40] Creaform (no date) HandyScan 3D, The truly portable metrology grade 3D-Scanner, [Online] Available at: https://www.creaform3d.com/sites/default/files/assets/brochures/files/handyscan3d_brochure_en_hq_21032017_2.pdf (accessed 27.01.18).
 - [41] Z Corporation (no date) Z Scanner[®] 800 High Resolution Handheld Scanner, [Online] Available at: <http://www.agile-manufacturing.com/files/products/zscanner-800.pdf> (accessed 27.01.18).
 - [42] L. Hu, D. Yun, Z. Lui, S. Du, Z. Zhang, Y. Bao, Effect of three-dimensional macrotexture characteristics on dynamic frictional coefficient of asphalt pavement surface, *Construct. Build. Mater.* 126 (2016) 720–729, <https://doi.org/10.1016/j.conbuildmat.2016.09.088>.
 - [43] A. Abellan, M. Jaboyedoff, T. Oppikofer, J.M. Vilaplana, Detection of millimetric deformation using a terrestrial laser scanner: experiment and application to a rockfall event, *Nat. Hazards Earth Syst. Sci.* 9 (2009) 365–372, <https://doi.org/10.5194/nhess-9-365-2009>.
 - [44] N. Micheletti, J.H. Chandler, S.N. Lane, Structure from Motion (SfM) Photogrammetry, *Geomorphological Techniques*, Chapter 2.2 (2015) ISSN 2047-0371. Available at: http://geomorphology.org.uk/geomorph_techniques (accessed 27.01.17).
 - [45] M.R. James, S. Robson, Straightforward reconstruction of 3D surfaces and topography with a camera: accuracy and geoscience application, *J. Geophys. Res.* 117 (2012) 1–17, <https://doi.org/10.1029/2011JF002289>.
 - [46] R. Leach, Introduction to surface topography, in: R. Leach (Ed.), *Characterisation of Areal Surface Texture*, Springer, London, 2013, pp. 1–13. ISBN-13:978364236457.
 - [47] G. Boscaino, F.G. Pratico, A classification of surface texture indices of pavement surfaces [Classification et inventaire des indicateurs de la texture superficielle des revêtements des chaussées], *Bull. Labor. Ponts Chaussées* 234 (2001). 17-34+123+125+127. ISSN: 1269-1496.
 - [48] ISO 13473-1: Characterisation of pavement texture by the use of surface profiles – Part 1: determination of mean profile depth. Geneva, Switzerland: International Organization for Standardization (2019) [Online] Available at <https://www.iso.org/obp/ui/#iso:std:iso:13473:-1:ed-2:v1:en> (accessed 03.01.18).
 - [49] LMI Technologies (ND), Gocator 2300 series all in one smart profile sensor, Available at: https://www.stemmer-imaging.co.uk/media/uploads/vision-systems/lmi/81/81688-LMI_Gocator_2300.pdf (accessed 18.03.18).
 - [50] H. Yaacob, N.A. Hassan, M.R. Hainin, M.F. Rosli, Comparison of sand patch test and multi laser profiles in pavement surface measurement, *J. Teknol.* 70 (4) (2014) 103–106, <https://doi.org/10.11113/jtv70.3497>.
 - [51] ISO 25178 Part 2, Geometrical product specification (GPS) – Surface texture: areal part 1: terms, definitions and surface texture parameters. International Organisation of Standardisation. (2012) [Online] Available at: <https://www.iso.org/standard/42785.html> (accessed 27.01.18).
 - [52] ISO 4288, Geometrical Product Specification (GPS) – Surface texture: Profile method – Rules and procedures for the assessment of surface texture, International Organization for Standardization, Geneva, Switzerland, 1996 (accessed 03.07.18).
 - [53] Y. Furukawa, J. Ponce, Accurate, dense, and robust multiview stereopsis, *IEEE Trans. Pattern Anal. Mach. Intell.* 32 (2010) 1362–1376, <https://doi.org/10.1109/TPAMI.2009.161>.
 - [54] LMI Technologies, Gocator Firmware 4.6, The Latest Features and Tools (ND), Available at: <https://lmi3d.com/products/gocator/firmware> (accessed 27.04.18).
 - [55] Girardeau-Montaut, D. Cloudcompare 3D point cloud and mesh processing software – open source project, Available at: <http://www.danielgm.net/cc/> (accessed 27.03.2018).
 - [56] D. Gubbins, *Time Series Analysis and Inverse Theory for Geophysicists*, Cambridge University Press, Cambridge, 2004.
 - [57] ISO 4287, Geometrical Product Specification (GPS)- Surface Texture: Profile Method – Terms, Definitions and Surface Texture Parameters, International Organisation of Standardisation, 1997 (accessed 27.01.18).
 - [58] P. Bloomfield, *Fourier Analysis of Time Series: An introduction*, Wiley-InterScience, New York, 2000.